DOI: 10.13009/EUCASS2023-915
Aerospace Europe Conference 2023 – 10TH EUCASS – 9TH CEAS

Flight Dynamics of Aircraft Incorporating the Semi-Aeroelastic Hinge

Huaiyuan Gu⋆, Fintan Healy, Djamel Rezgui, Mark Lowenberg, Jonathan Cooper
Department of Aerospace Engineering, University of Bristol
Queen's Building, University Walk, Bristol BS8 1TR
huaiyuan.gu@bristol.ac.uk
⋆Corresponding author

Abstract
This paper investigates the dynamic behaviour of an aircraft incorporating a semi-aeroelastic hinge (SAH), a hinge device that enables wingtips to be released during gusts and manoeuvres to alleviate the aerodynamic loads, whilst remaining locked in cruise to obtain the optimum aerodynamic shape. A six degree of freedom flight mechanics model incorporating flexible wings and SAH devices is formulated to evaluate dynamic responses of the aircraft to gusts and control surface inputs. The results are compared between models with various hinge conditions and wingtip sizes, where approximately 50% and 20% reduction in the gust and manoeuvre loads are observed once the hinge are released. Furthermore, aircraft dynamic modes are computed and compared between the models with various wing flexibility and hinge positions. It is shown that a SAH device is able to reduce both roll damping and pitch stiffness leading to approximately 50% and 15% improvement in the roll and pitch rates.

1. Introduction

Much recent interest has focused on employing high aspect ratio wings to modern aircraft design, with the aim of the drag reduction and thereby obtaining better performance. However, the increased wingspan is not without drawbacks, and the chief among these is attributed to the airport gate size restrictions. Folding wingtips have been employed to overcome this problem, such as the latest Boeing 777-X model [1] which is able to fold up its wingtips after landing, and unfold and lock the hinges before takeoff. A further advancement has been emerged in recent years to focus on the development of an in-flight hinge control system known as the semi-aeroelastic hinge (SAH) [2, 3, 4, 5], which enables the wingtips to be released in-flight to alleviate gust and manoeuvre loads, whilst remaining locked in cruise to maintain the optimum aerodynamic shape, as illustrated in Figure 1. A large body of work has been conducted to investigate the load alleviation performance and dynamic stability of the device [6, 7, 8, 9], whereas not many of these studies concern the impact of the device configuration such as the hinge position upon the overall aircraft dynamics.

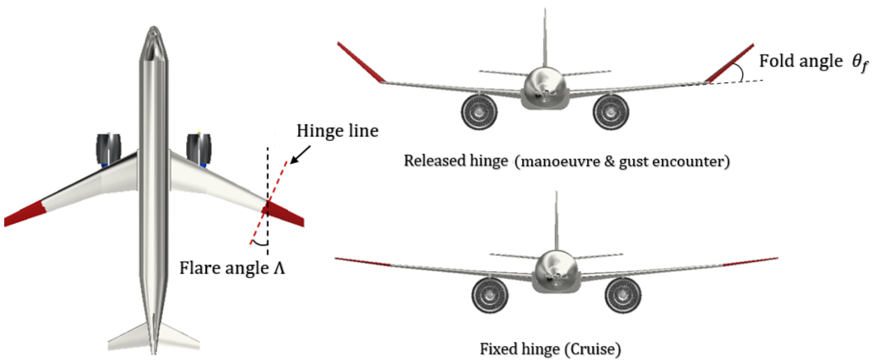

Figure 1: Schematic representation of the semi-aeroelastic hinge (SAH).

DOI: 10.13009/EUCASS2023-915

Unlike conventional folding wingtips, as employed on the Boeing 777X, the semi-aeroelastic hinge (SAH), is at an angle to the oncoming flow direction, known as the flare angle, Λ, as shown in Figure 1, which indicates a positive Λ. With a positive flare angle, Λ, the local angle of attack on the folding wingtip reduces with the fold angle, θ_f. At small fold angles, the change in the local angle of attack can be related to the fold angle, θ_f, as [10]:

$$\Delta\alpha = -\arctan(\sin\Lambda\tan\theta_f) \tag{1}$$

And in cases of large fold angle the relationship between the folding angle, θ_f, and local angle of attack becomes [11]:

$$\Delta\alpha = -\sin\Lambda\sin\theta_f \tag{2}$$

When the hinge is released in-flight, the wingtip folds up towards a steady fold angle, known as the coast angle, where the aerodynamic forces and moments are balanced with those caused by the wingtip weight. Research has been conducted to investigate the significance of the flare angle, Λ, on the dynamic behaviours and load alleviation performance of the device [8, 12, 13]. It has been shown that a greater flare angle, Λ, may result in a better load alleviation due to the rapid change of aerodynamic loads on the wingtip with the fold angle, however, the dynamic stability, such as the flutter speed will be compromised [8]. Sizing of a high aspect ratio wing incorporating a SAH was performed [14] to evaluate the impact of the device on the wing weight and overall aircraft performance, where an approximately 30 % reduction in the wing weight was seen owing to the presence of the SAH leading to 5 % increase in aircraft range.

Numerical studies have been conducted to reveal the effect of folding wingtips on the flight dynamics including the stability derivatives, damping and frequencies of the aircraft modes [15, 16]. To obtain the greater understanding of the impact of the SAH device on the flight handling quality, a set of experimental analyses were conducted by the current authors [17] to measure and compare the aerodynamic and control derivatives of an aircraft model with various hinge configurations. It shows that the SAH device causes little impact on the longitudinal flight dynamics of an aircraft, whereas more profound influences were seen on the lateral-directional motions, especially when the wing is relatively rigid [18]. This phenomenon was also been experimentally revealed by Healy et al. [19], where a significantly improvement in the roll performance of a high aspect ratio wing once the hinge was released, attributing to the reduction of the roll damping.

This paper develops a full flight mechanics model of an aircraft with flexible wings including both longitudinal, and lateral-directional dynamics, to investigate the influences of the semi-aeroelastic hinge (SAH) device on the flight mechanics and flight handling qualities (FHQ). The detailed model formulation is described in section 2. The flight mechanics model is then employed to explore dynamic responses of an A321-like aircraft model incorporating high aspect ratio wings and SAH with various hinge configurations, see section 3.1 and 3.2. Finally, the impact of the SAH device on fight handling qualities is examined in section 4, by comparing the aircraft modal characteristics with a range of wing flexibility and hinge configurations.

2. Flight mechanics model formulation

This section describes formulation of the flight mechanics of the aircraft model incorporating semi-aeroelastic hinge (SAH). In this study, the aerodynamic forces are calculated based on strip theory. The flexibility of the model is only considered for the main wings, whereas the rest of the airframe i.e. fuselage and empennage are assumed to be rigid. Consider an aircraft incorporating flexible wings, the elastic displacement, Z_w, and twist, θ_w, of the main wing can be expressed in the form of [20]:

$$Z_w(x, y, t) = \sum_{n=1}^{3} -\phi_{bi}q_{bi} + \sum_{n=1}^{2} \phi_{ti}q_{ti}(x - x_f) \tag{3}$$

$$\theta_w(x, y, t) = \sum_{n=1}^{j} \phi_{ti}q_{ti} \tag{4}$$

where x, y and z indicate positions of arbitrary points on the wing described in the conventional aircraft body-axis as illustrated in Figure 2. q_{bi} and q_{ti} in Eq. 3 are the corresponding generalised coordinates for the wing bending and

DOI: 10.13009/EUCASS2023-915

torsion. $x - x_f$ represents the chordwise distance of an arbitrary point on the wing to the elastic axis (mid-chord). In this work, five elastic modes are considered in the wing kinematics including three bending and two torsional modes with following assumed shapes:

$$\phi_{b1} = (\frac{y}{b})^2 \quad \phi_{b2} = (\frac{y}{b})^3 \quad \phi_{b3} = (\frac{y}{b})^4 \quad \phi_{t1} = (\frac{y}{b}) \quad \phi_{t2} = (\frac{y}{b})^2 \tag{5}$$

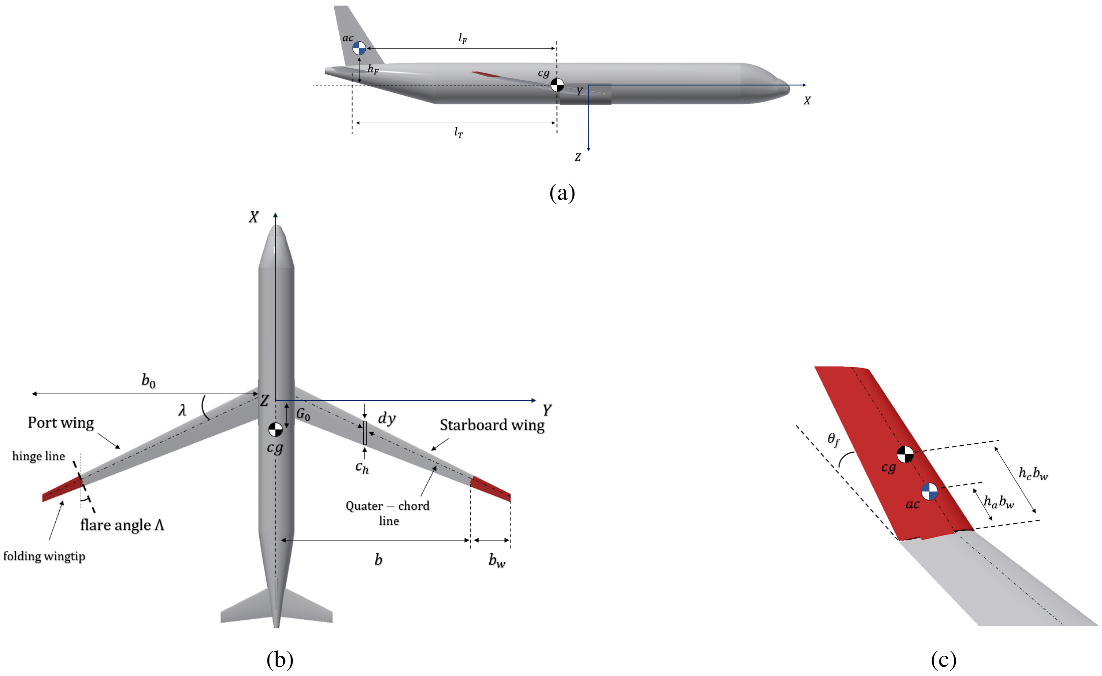

Figure 2: Schematic drawing of aircraft model incorporating folding wingtips.

The classical Lagrangian approach is employed to obtain the equations of motions so that:

$$\frac{d}{dt}\frac{\partial T}{\partial \dot{q}_i} + \frac{\partial U}{\partial q_i} = \sum Q_i \tag{6}$$

where T and U are the kinetic energy and potential energy of the entire system. Q_i is the generalised forces. For the model incorporating flexible wings and folding wingtips (FWT), the total kinetic energy, T, consists of the energy due to the wing fluctuation, T_w, and rigid motions of the aircraft, T_a, which take the form:

$$T = T_w + T_a \tag{7}$$

$$T_w = \frac{1}{2}\rho_m \iint_A \dot{Z}_w(x, y, t)\, dxdy \tag{8}$$

$$T_a = \frac{1}{2}M_a\dot{X}^2 + \frac{1}{2}M_a\dot{Y}^2 + \frac{1}{2}M_a\dot{Z}^2 + \frac{1}{2}I_{XX}p^2 + \frac{1}{2}I_{YY}q^2 + \frac{1}{2}I_{ZZ}r^2 + \frac{1}{2}I_f\dot{\theta}_f^2 \tag{9}$$

where X, Y and Z describe the position of the aircraft. p, q, and r indicate the aircraft roll, pitch and yaw rates. ρ_m is the area density of the wing i.e. ratio between the wing mass and area. M_a, I_{XX}, I_{YY}, and I_{ZZ} are the mass and moment of inertia of the aircraft. The potential energy, U_E, of the wing due to the elastic bending, twisting and wingtip flapping can be written as:

DOI: 10.13009/EUCASS2023-915

$$U_E = \frac{1}{2}\int_0^b EI(\phi_b'' q_{bi})^2\, dy \; + \frac{1}{2}\int_0^b GJ(\phi_{ti}' q_{ti})^2\, dy \; + m_f g(l_g \sin\theta_f + Z_{wh}) \tag{10}$$

where m_f is the wingtip mass. l_g is the perpendicular distance between the c.g. of the wingtip and hinge line. Z_{wh} is the vertical displacement of the hinge. The generalised force Q_j is calculated as the product of the force, f_j, acting on the system and the partial differentiation of the corresponding virtual displacement, r_j, with respect to generalised coordinate, q_i.

$$Q = \sum Q_j = f_j \frac{\partial r_j}{\partial q_i} \tag{11}$$

Therefore the overall generalised force Q can be calculated as the sum of the components due to the aerodynamic forces acting on the wings (starboard and port), $Q_{wing,R}$ and $Q_{wing,L}$, horizontal stabiliser, Q_{tail}, vertical fin, Q_{fin}, gravitational force, Q_{Grav}, engine thrust, Q_{thrust} and external forces attributed to the gust and control surfaces, Q_e:

$$Q = Q_{wing,L} + Q_{wing,R} + Q_{tail} + Q_{fin} + Q_{Grav} + Q_{thrust} + Q_e \tag{12}$$

For the generalised force on the starboard wing,

$$Q_{wing,R} = \int_0^b dL_{inner,R} \frac{\partial r_{inner,R}}{\partial q_j} + \int_b^{b+b_w} dL_{fwt,R} \frac{\partial r_{fwt,R}}{\partial q_j} \tag{13}$$

where b_w is wingtip span, and the incremental lift for the starboard wing, $dL_{inner,R}$ can be written as:

$$dL_{inner,R} = \overline{q_R} a_0 (\alpha_0 + \frac{W}{U} + \frac{V\gamma}{U} + \frac{\sum \phi_{bi,R}\dot{q}_{bi,R}}{U} + \phi_{ti,R} q_{ti,R} + \underbrace{\sum \phi_{bi,R}' q_{bi,R} \sin\lambda}_{\text{twist by bending}}) c(y)\, dy \tag{14}$$

And

$$dL_{fwt,R} = \overline{q_R} a_0 (\alpha_{hR} - \frac{V \sin\theta_{f,R}}{U} - \sin\Lambda \sin\theta_{f,R} - \frac{\dot{\theta}_{f,R}(y - y_h)}{U}) c(y)\, dy \tag{15}$$

where U, V, W are the forward, side and heave speeds of the model respectively. γ represents the dihedral angle. a_0 is the lift slope of the wing, $\overline{q_R}$ is the dynamic pressure acting on the starboard wing, $\theta_{f,R}$ indicates the fold angle of the starboard wingtip and α_{hR} is the effective angle of incidence at the starboard hinge. Similarly a set of expressions for the incremental lift on the port wing can be obtained as:

$$dL_{inner,L} = \overline{q_L} (\alpha_0 + \frac{W}{U} - \frac{V\gamma}{U} + \frac{\sum \phi_{bi,L}\dot{q}_{bi,L}}{U} + \phi_{ti,L} q_{ti} + \sum \phi_{bi,L}' q_{bi,L} \sin\lambda) c(y)\, dy \tag{16}$$

$$dL_{fwt,L} = \overline{q_L} (\alpha_{hL} + \frac{V \sin\theta_{f,L}}{U} - \sin\Lambda \sin\theta_{f,R} - \frac{\dot{\theta}_{f,R}(y - y_h)}{U}) c(y)\, dy \tag{17}$$

The aerodynamic forces on the horizontal tail and vertical fin can be written as:

$$L_{tail} = \overline{q_T} S_T [a_T (\frac{W + l_T q}{U}(1 - \varepsilon)) + a_\eta \eta_e)] \tag{18}$$

DOI: 10.13009/EUCASS2023-915

$$L_{fin} = \overline{q_F} S_F [a_F(-\frac{V}{U} - \frac{h_F p}{U} + \frac{l_F r}{U}) + a_\zeta \zeta)] \tag{19}$$

where S_T, S_F, l_T, h_F, l_F are the areas and moment arms of the aerodynamic forces acting on the horizontal tail and fin, see figure 2. η_e, ζ are the elevator and rudder deflections, and a_η, and a_ζ are their corresponding lift slopes. ε is the downwash angle on the tailplane. p, q, r are the roll, pitch and yaw rate respectively. Hence, the full equations of motion of the aircraft can be obtained by substituting Eq. 7 to 19 into Eq. 6.

3. Numerical Results

In this section, the equations of motion derived in section 2 are solved by direct integration using MATLAB ode functions [21], where the responses are computed in the time domain. The dynamic behaviour of an A321-like aircraft model incorporating SAH is considered in this study, where the details of the planform are given in Table 1. The model is trimmed under flight speed of 220 m/s at the altitude of 36000 ft, and the vertical gust and control surface inputs are then introduced to the model. The results are compared between various hinge configurations to assess the impact of the SAH on aircraft dynamics.

Table 1: Summary of parameters of the aircraft model.

Model geometric parameters	**Value**
Wingspan(b_0)	48.1m
Wing surface area(S_W)	122 m^2
Taper ratio	0.24
Aspect ratio (AR)	19
Dihedral(γ)	5°
Quater-chord sweep(λ)	24°
Wing setting angle (α_0)	4°
Aileron position($y_{a1} - y_{a2}$)	0.7b - 0.9b
Flare angle(Λ)	20°
Tailplane surface area(S_T)	35 m^2
Tailplane setting angle (i)	-2°
Tail moment arm (l_T)	27m
Fin surface area(S_T)	30 m^2
Fin moment arm (l_F)	25m
cg position (relative to the wing root)	4.2m
Mass configurations	
Model mass (m)	50000 kg
Wing area density (ρ_m)	60 kg/m^2
Roll inertia (I_x)	1.267×10^6 kg.m^2
Pitch inertia (I_y)	2.441×10^6 kg.m^2
Yaw inertia (I_z)	3.925×10^6 kg.m^2

3.1 Response to gust

In the case considered, the aircraft was assumed to experience a vertical gust in the form of one minus cosine (1MC), with gust length, L_g, of 214 metres, and peak gust velocity of 7.9 m$/s$. The gust profile was defined as,

$$W_g = \begin{cases} \frac{W_{g0}}{2}(1 - \cos\frac{2\pi U(t-t_0)}{L_g}), & \text{for } t_0 < t < \frac{l_g}{U} \\ 0, & \text{for } t > \frac{l_g}{U} \end{cases} \tag{20}$$

where t_0 is the time of gust onset, which was chosen to be 5s as shown in Figure 3(a). Note that on the tailplane, an additional time delay, Δt, was added to t_0 to replicate the penetration effect of the gust. The Δt was calculated as,

$$\Delta t = \frac{l_s}{U} \tag{21}$$

DOI: 10.13009/EUCASS2023-915

where l_s is the distance between *ac* of the wing and that of the tailplane. The gust responses were computed for the hinge locked case and two free hinge cases, where the size of the folding wingtips, η_f, were 20% and 30% of the wingspan. The responses of the aircraft and wing motions are shown in Figure 3. It is clear that the models with free hinge exhibited significantly less root bending moment, whereas the impact on the root torque is relatively small. A better load alleviation performance was seen in the model with greater folding wingtips, η_f, due to the significant reduction in the lift generated on the outboard wingspan. Furthermore, it can be seen that the influence of the hinge condition on the gust responses of the overall aircraft dynamics was minimal.

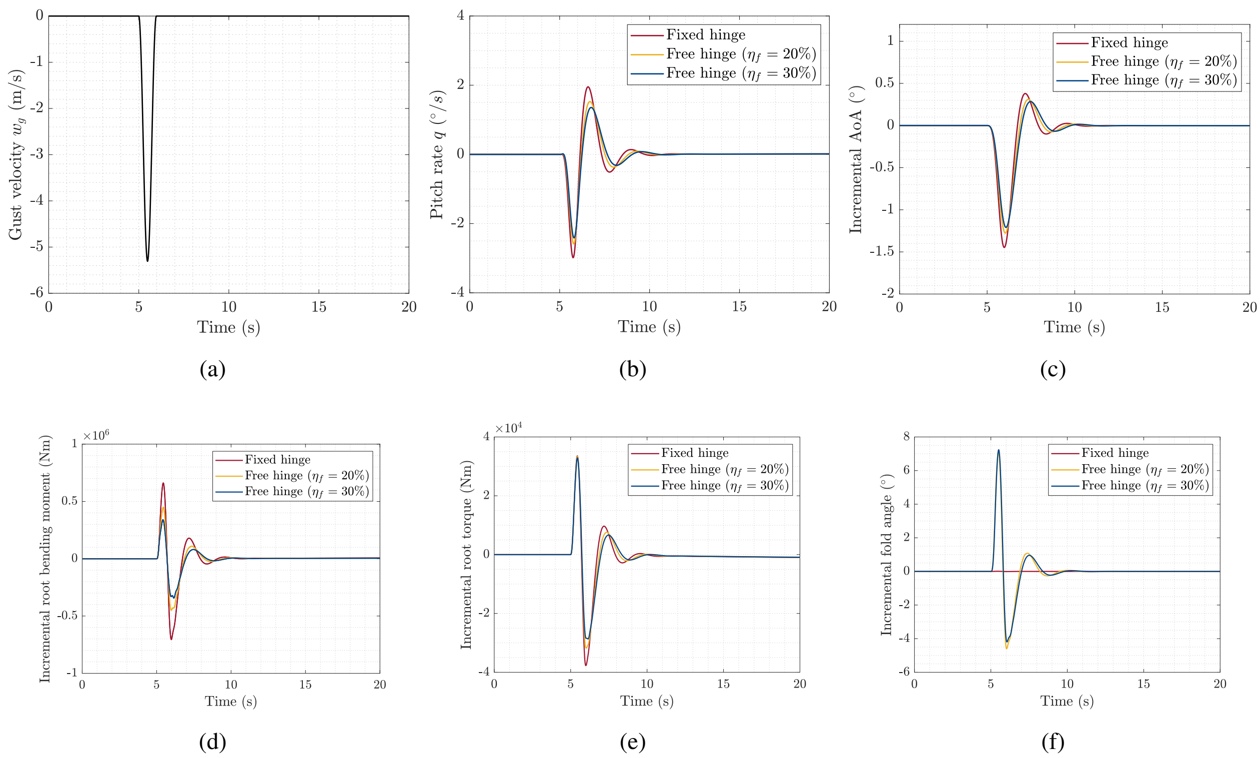

Figure 3: Dynamic responses to the vertical gust (a) gust input (b) pitch rate (c) angle of attack (d) wing root bending moment (e) wing root torque (f) fold angle.

3.2 Response to control inputs

In this section, control inputs are applied to the three models i.e. fixed hinge model, and two free hinge models with $\eta_f = 20\%$ and $\eta_f = 30\%$, respectively. The longitudinal dynamic responses of the models are investigated by applying an elevator step input, where the responses of the angle of attack (*AoA*), pitch rate, q, and wing motions are evaluated as shown in Figure 4. It can be seen that the *AoA*, increases linearly with the elevator input, and the free hinge models exhibited greater pitch rate, q, compared to the fixed hinge model due to the change of the aerodynamic centre of the wing after the wingtips are released. Furthermore, less root bending moment was seen during the pitch manoeuvre for the free hinge cases compared to that of the fixed hinge model, due to the positive fold angles, θ_f, leading to the reduced the local *AoA* on the wingtips. It was also seen that the free hinge model shows higher root torque during the manoeuvre than the fixed hinge model. This is due to the presence of the wing sweep angle which introduced bend-twist coupling to the wing. The model manoeuvre with free hinge condition causes the reduced lift on the wingtips, whereas the higher aerodynamic forces were acting on the inboard wing. Although the root bending moment was reduced due to the reduction in the moment arm of the lift, the lower wing bending in turn reduced the coupled nose-down twist, leading to a higher torque at the wing root. Figure 5 shows the dynamic responses of the aircraft motion, to an aileron step input. The aileron deflection was first increased to -2°, then held for the rest of the simulation, as shown in Figure 5 (a). It's clear that the responses of the roll motions were non-oscillatory. The roll angle increased linearly with the aileron angle, and the roll rate gradually decreased under the constant aileron deflection, shown in Figure 5 (b). This was mainly due the restoring roll moment attributing to the presence of the wing dihedral, sweep angle, and vertical fin which stablised the lateral motion of the aircraft [22]. It can be seen that the free hinge models exhibited significantly higher roll rate compared to that of the fixed hinge model due to the reduction in the roll damping, see

DOI: 10.13009/EUCASS2023-915

section 4, although it also led to a slightly higher root bending moment occurring in the free hinge models. The aircraft responses to a -2° rudder step input are shown in Figures and 6. Both yaw rate, r, and yaw angle, ψ, increased with rudder deflection shown in Figure 6 (b) and (c). Significant fluctuation was seen in the time history plot, attributed to the present of the dutch-roll mode. It can be seen that the impact of the hinge conditions on the responses of rudder input was relatively small compared to that of the aileron and elevator inputs.

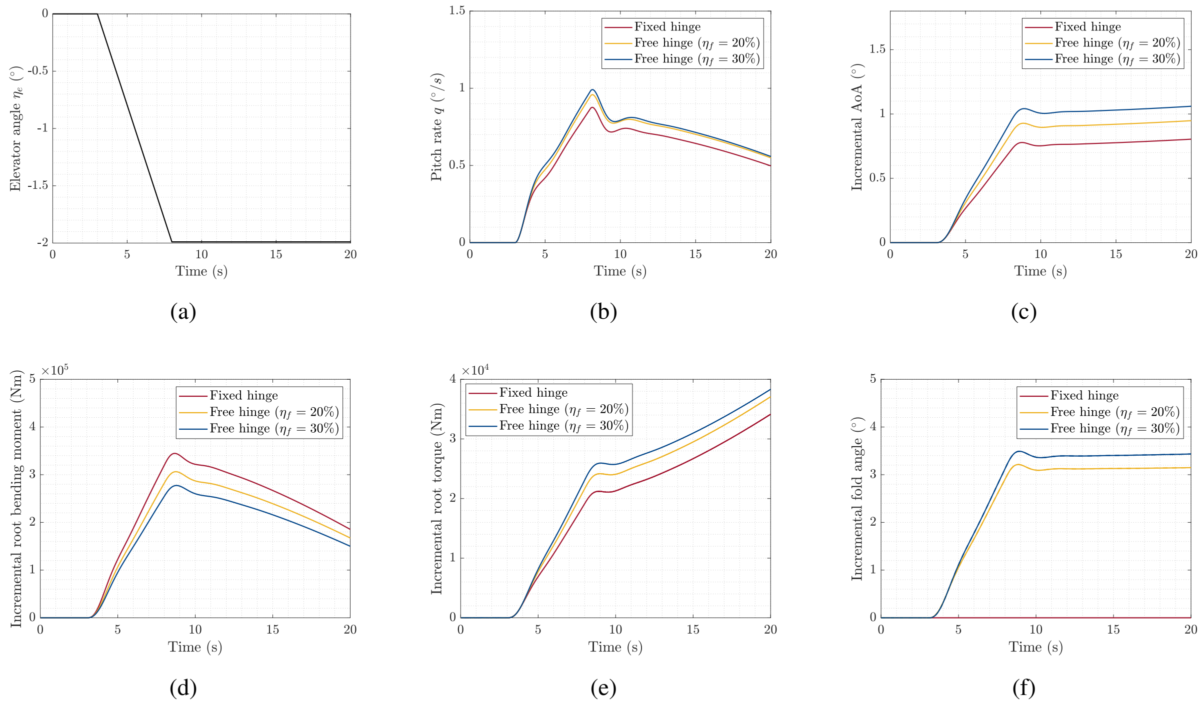

Figure 4: Dynamic responses to the elevator input (a) elevator step input (b) pitch rate (c) angle of attack (d) wing root bending moment (e) wing root torque (f) fold angle.

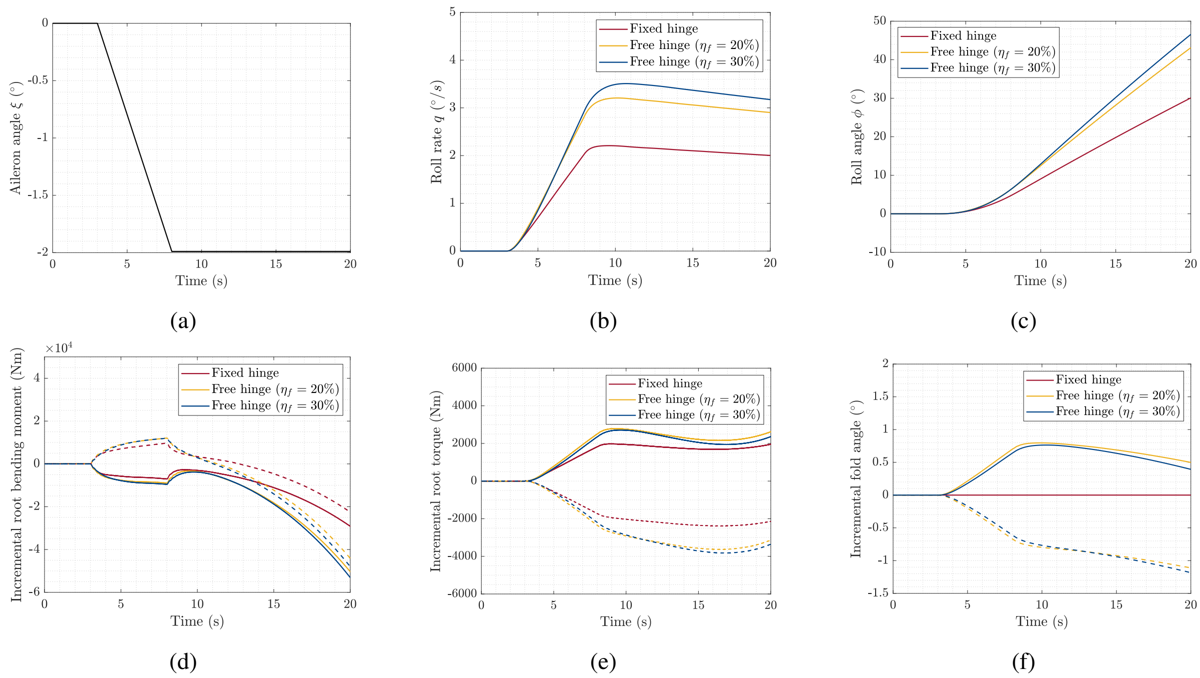

Figure 5: Dynamic responses to the aileron input (a) aileron step input (b) roll rate (c) roll angle (d) wing root bending moment (e) wing root torque (f) fold angle. The solid and dashed lines indicate the responses of the starboard and port wings.

DOI: 10.13009/EUCASS2023-915

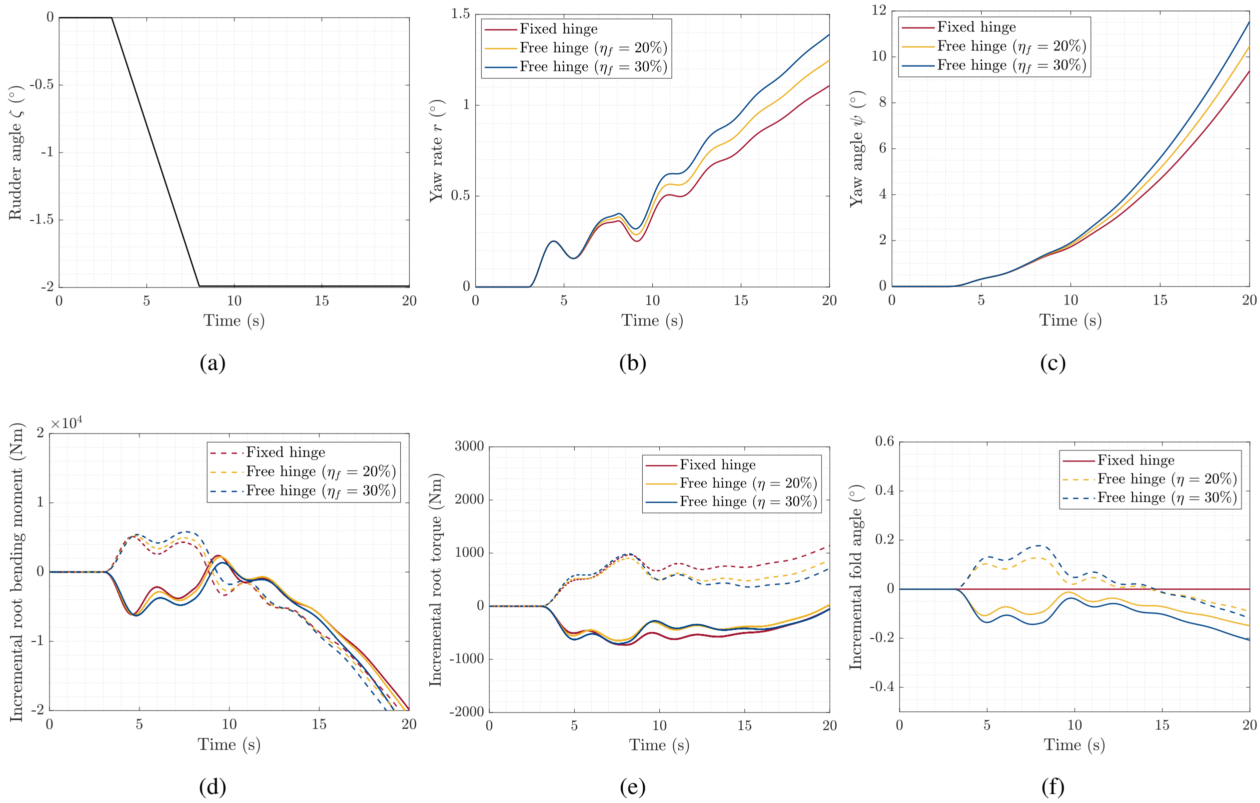

Figure 6: Dynamic responses to the rudder input (a) rudder step input (b) yaw rate (c) yaw angle (d) root bending moment (e) root torque (f) fold angle. The solid and dashed lines indicate the responses of the starboard and port wings.

4. Aircraft modes

Figure 7 (a) and (b) show the root locus of the short-period mode of the free hinge models with a range of folding wingtip sizes, η_f, and wing flexibility i.e. bending, EI, and torsional, GJ, rigidity. Analysis was performed with the wings with three different levels of rigidity, and for each selected EI and GJ, the system roots were calculated for η_f, varying from 10% to 40% of the wingspan, shown in Figure 7. It was found that the imaginary part of the short-period poles reduces with increasing folding wingtip size, η_f, whereas the variation of the real part caused by the change of η_f was relatively small, particularly for the wing with a relatively high bending rigidity, EI. Furthermore, with decreasing EI, the short-period poles shifted towards the right on the complex plane. The impact caused by the change of GJ was found to be opposite to that of EI, where the decrease in GJ, resulting in the roots moving towards the left.

The damping ratio, ζ, and undamped natural frequency, ω_s of the short-period mode were calculated from the poles, which are traditionally considered as one of indicators of the longitudinal flight handling quality. The results were then compared to the pilot opinion contour, known as the thumb print criterion [22], shown in Figure 8. It was found that the undamped natural frequency ω_s reduces significantly with increasing size of the folding wingtips, η_f, due to the change of the aerodynamic centre of the main wings. Figure 9 compares the locations of the mean aerodynamic chord (*mac*) and resulting movements of the aircraft neutral point (NP) of the fixed and free hinge models with $\eta_f = 20\%$ and $\eta_f = 30\%$. It can be seen that with increasing size of folding wingtips,η_f, *N.P.* moves toward the *cg*, resulting in the reduction in the stability margin, and thereby, a decreased pitching stiffness. The reduction in the short-period natural frequency, ω_s, is also reflected in the time history of the response to the elevator input, as shown in Figure 4, where a higher pitch rate was seen in the model with greater folding wingtips, η_f. Furthermore, it was found that the increase in the wing bending rigidity, EI, resulted in a reduction in the short-period frequency, ω_s, and increase in the damping ratio, ζ. While an increase in the torsional rigidity, GJ, led to an increased frequency, ω_s, and reduction in the damping ratio, ζ.

DOI: 10.13009/EUCASS2023-915

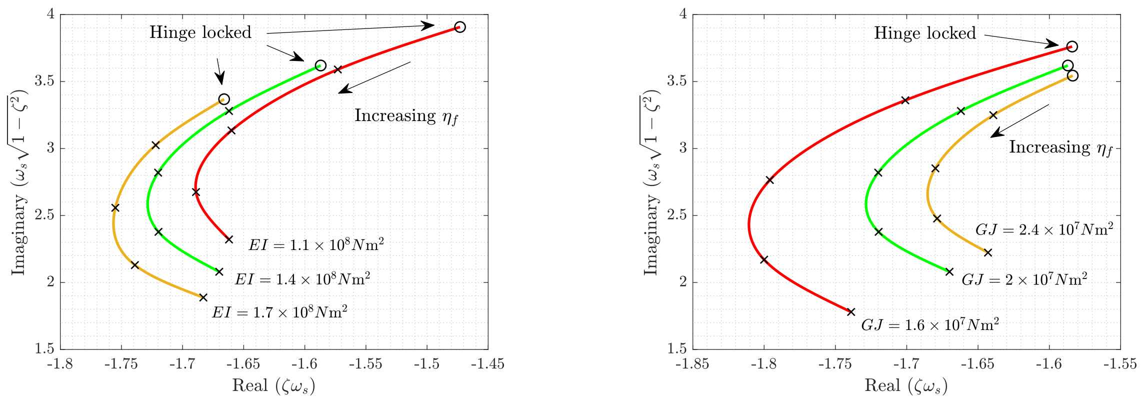

(a) (b)

Figure 7: Root locus of Short-period mode of the model with various folding wingtip sizes, η_f, and (a) wing bending rigidity, EI; (b) wing torsional rigidity, GJ.

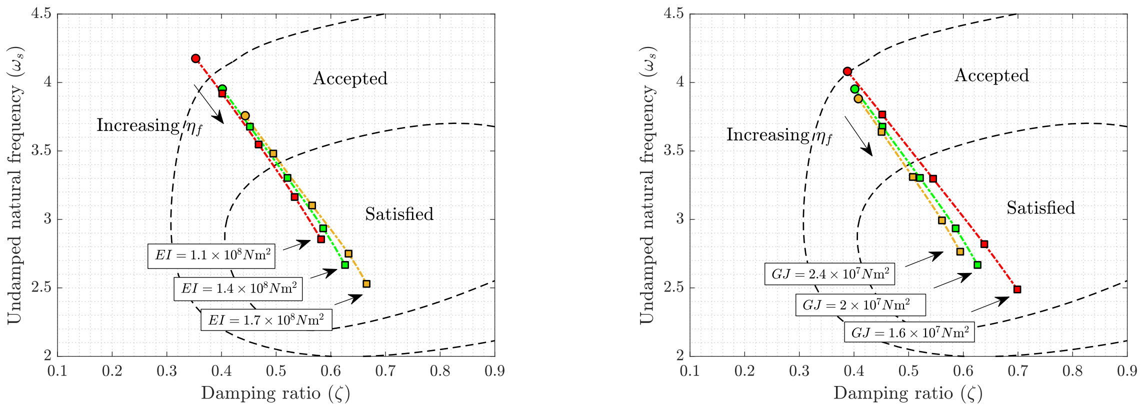

(a) (b)

Figure 8: Undamped natural frequencies and damping ratios of short-period mode of the model with various folding wingtip sizes and (a) wing bending rigidity, EI; (b) wing torsional rigidity, GJ.

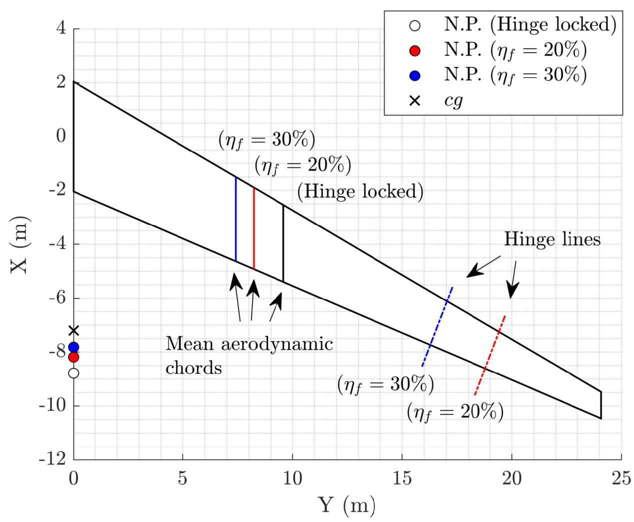

Figure 9: Variation of the positions of mean aerodynamic chord and control fixed neutral point (*N.P.*) of the models incorporating various sizes of folding wingtips, η_f.

DOI: 10.13009/EUCASS2023-915

The root locus of the Phugoid modes is presented in Figures 10. The change of the size of folding wingtips, η_f, and wing flexibility, caused significant impact on both real and imaginary parts of the poles. It shows that the wing exhibiting low bending rigidity, EI, and large folding wingtip, η_f, resulted in a higher imaginary part, and reduced real part of the poles. When the torsional rigidity, GJ, was increased, the entire root locus was rotated anti-clock wise, where the imaginary part of the pole decreased for $\eta_f > 20\%$, and increased for $\eta_f < 20\%$.

Figure 12 shows the root locus of the Dutch roll mode, where the impact of both wing flexibility and folding wingtip are very small. It was found that the increase in folding wingtip size η_f and wing bending rigidity, EI, resulted in a slight reduction of the imaginary part, whereas no clear correlation was seen between the torsional rigidity, GJ, and the poles. Figure 11 depicts the the root of the roll subsidence mode against the wing flexibility. Since the roll mode is non-oscillatory, the imaginary parts of the poles were equal to zero. The magnitude of the real part of the poles reduces significantly with increasing folding wingtip sizes, η_f, indicating significantly reduction of the roll damping. The conclusion was consistent with the time history plot shown in Figure 5, where the higher roll rate was seen in the model with greater, η_f. For the cases considered, no obvious effect of wing flexibility was seen on the roll motion. Furthermore, it was shown that the influences of SAH on the aircraft spiral mode is negligible, as suggested in Figures 13.

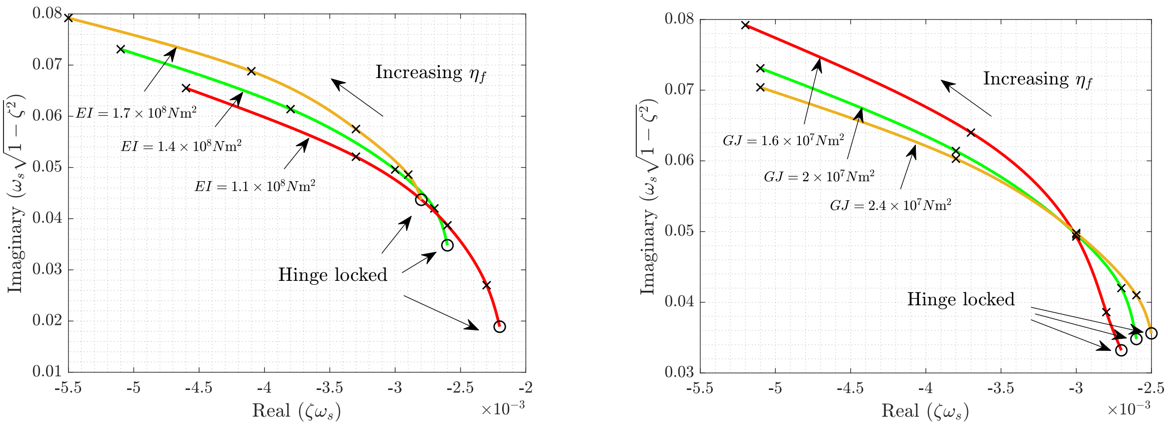

(a) (b)

Figure 10: Root locus of Phugoid mode of the model with various folding wingtip sizes, η_f, and wing bending rigidity, EI; (b) wing torsional rigidity, GJ.

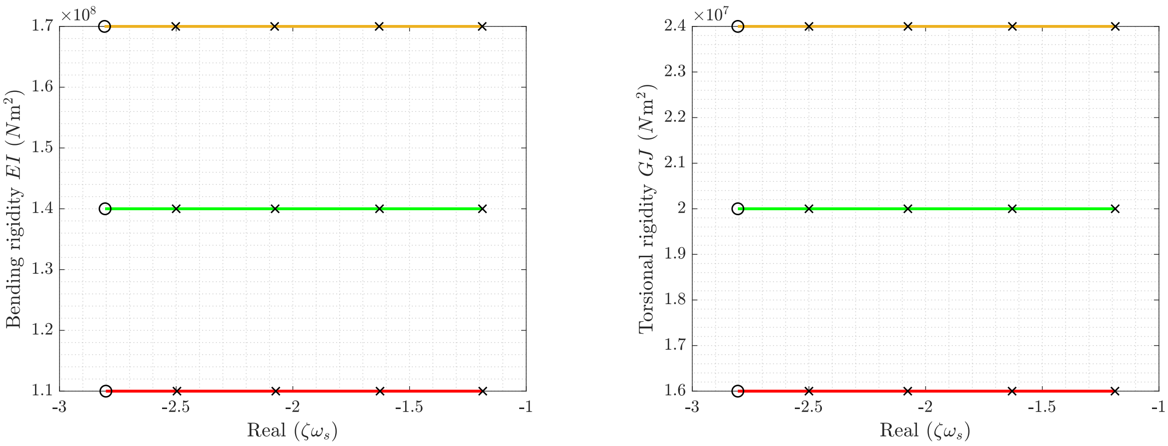

(a) (b)

Figure 11: Root locus of roll mode of the model with various folding wingtip sizes, η_f, and wing bending rigidity, EI; (b) wing torsional rigidity, GJ.

DOI: 10.13009/EUCASS2023-915

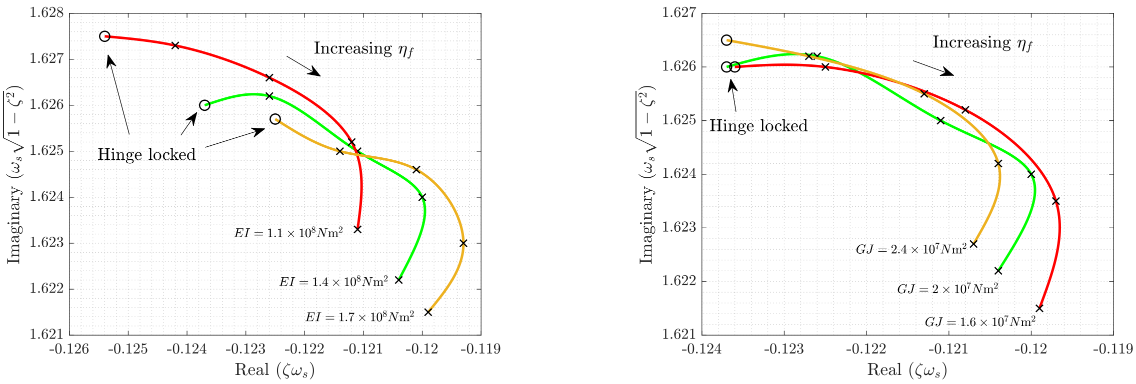

(a) (b)

Figure 12: Root locus of Dutch-roll mode of the model with various folding wingtip sizes, η_f, and wing bending rigidity, EI; (b) wing torsional rigidity, GJ.

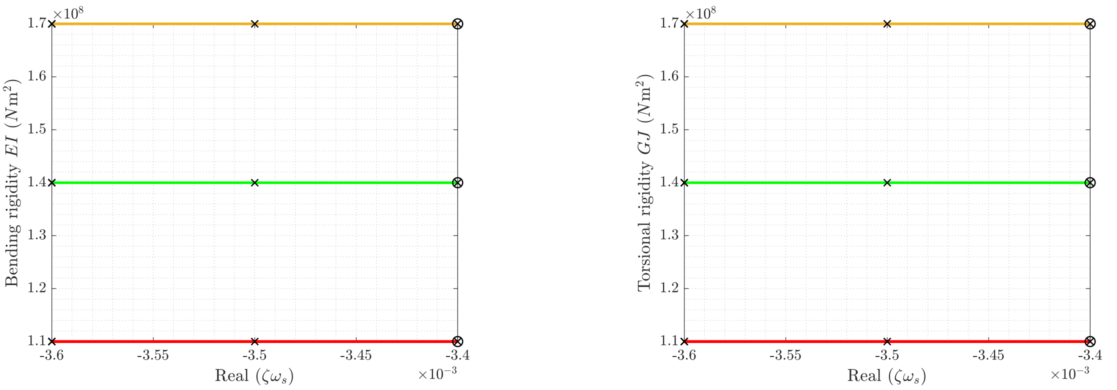

(a) (b)

Figure 13: Root locus of Spiral mode of the model with various folding wingtip sizes, η_f, and wing bending rigidity, EI; (b) wing torsional rigidity, GJ.

5. Conclusions

In this study, a flight mechanics model of an A321-like aircraft incorporating a semi-aeroelastic hinge (SAH) was developed, and the model was employed to investigate dynamic responses to gust and control surface inputs. The results were compared for various hinge configurations, to assess the impact of the SAH upon the flight mechanics of the aircraft. It was shown that release the hinge will lead to the reduction in the stability margin of the aircraft, causing higher pitch rate for a given elevator input compared to that of the fixed hinge case. A significant improvement in the roll rate was observed in the free hinge model, owing to the significant reduction of the roll damping after the hinge was released. The results also suggest that a further improvement in the roll rate can be achieved by implementing a larger folding wingtips. Furthermore, the impact of the wing flexibility for such wing configuration was investigated and it was found that the reduction in the wing bending rigidity, EI, resulted in a reduced damping and increased frequency of the short-period mode, while the change in the wing torsional rigidity, GJ, led to an opposite effect. Whereas no significant impact of wing flexibility was observed on the lateral-directional dynamics in the cases considered in the study.

6. Acknowledgments

The authors acknowledge funding from the DAWS (Development of Advanced Wing Solutions) project (No. 113288) supported by the ATI Programme, a joint Government and industry investment to maintain and grow the UK's competitive position in civil aerospace design and manufacture. The programme, delivered through a partnership between the Aerospace Technology Institute (ATI), Department for Business, Energy and Industrial Strategy (BEIS) and Innovate UK, addresses technology, capability and supply chain challenges.

DOI: 10.13009/EUCASS2023-915

References

[1] Mathew Lassen, Chad Douglas, Kelly Thomes Jones, and Terence Boyd Kenning. *Wing Fold Controller*. Office, European Patent, 2018. EP2727829B1.

[2] Thomas Wilson, Andrea Castrichini, Alvaro Azabal, Je Cooper, Rafic Ajaj, and Martin Herring. Aeroelastic behaviour of hinged wing tips. In *International Forum of Aeroelasticity and Structural Dynamics*, Como, Italy, 2017.

[3] Claudio Conti, Francesco Saltari, Franco Mastroddi, Thomas Wilson, and Andrea Castrichini. Quasi-steady aeroelastic analysis of the semi-aeroelastic hinge including geometric nonlinearities. *Journal of Aircraft*, pages 1–11, 2021.

[4] Thomas Wilson, James Kirk, John Hobday, and Andrea Castrichini. Small scale flying demonstration of semi aeroelastic hinged wing tips. In *International Forum on Aeroelasticity and Structural Dynamics*, Savannah, Georgia, USA, 2019.

[5] T. Wilson, A. Azabal, A. Castrichini, J.E. Cooper, R. Ajaj, and M. Herring. Aeroelastic behaviour of hinged wing tips. *International Forum on Aeroelasticity and Structural Dynamics*, 2017.

[6] Ronald C. M. Cheung, Djamel Rezgui, Jonathan E. Cooper, and Thomas Wilson. Testing of a hinged wingtip device for gust loads alleviation. *Journal of Aircraft*, 55(5):2050–2067, 2018.

[7] J. E. Cheung. R. C. M., Rezgui. D. Cooper and Wilso. T. Testing of a hinged wingtip device for gust loads alleviation. *Journal of Aircraft*, 55(5):2050â2067, 2018.

[8] A. Castrichini, J. E. Cooper, T. Wilson, A. Carrella, and Y. Lemmens. Nonlinear negative stiffness wingtip spring device for gust loads alleviation. *Journal of Aircraft*, 54(2):627–641, 2017.

[9] A. Castrichini, V. Hodigere Siddaramaiah, D. E. Calderon, J. E. Cooper, T. Wilson, and Y. Lemmens. Nonlinear folding wing tips for gust loads alleviation. *Journal of Aircraft*, 53(5):1391–1399, 2016.

[10] A. Castrichini, V. Hodigere Siddaramaiah, D.E. Calderon, J.E. Cooper, T. Wilson, and Y. Lemmens. Preliminary investigation of use of flexible folding wing tips for static and dynamic load alleviation. *The Aeronautical Journal*, 121(1235):73â94, 2017.

[11] William Blunt, Fintan Healy, Ronald C. Cheung, Mark H. Lowenberg, and Jonathan E. Cooper. Trailing edge tabs on folding wingtips (fwts) for aircraft roll control. *AIAA SCITECH 2022 Forum*, 2022.

[12] Fintan Healy, Ronald C. Cheung, Djamel Rezgui, and Jonathan E. Cooper. Nonlinear stability analysis and experimental exploration of limit cycle oscillations with flared folding wingtips. *AIAA SCITECH 2022 Forum*, 2022.

[13] Fintan Healy, Ronald C. Cheung, Djamel Rezgui, and Jonathan E. Cooper. Experimental analysis of the behaviour of flared folding wingtips with sideslip angle. *International Forum on Aeroelasticity and Structural Dynamics (IFASD)*, 2022.

[14] Gu Huaiyuan, Healy Fintan, Rezgui Djamel, and Cooper Jonathan. Sizing of high-aspect-ratio wings with folding wingtips. *Journal of Aircraft*, 60(2):461–475, 2023.

[15] Ajaj Rafic M. Flight dynamics of transport aircraft equipped with flared-hinge folding wingtips. *Journal of Aircraft*, 58(1):98–110, 2021.

[16] A. Castrichini, T. Wilson, F. Saltari, F. Mastroddi, N. Viceconti, and J. E. Cooper. Aeroelastics flight dynamics coupling effects of the semi-aeroelastic hinge device. *Journal of Aircraft*, 57(2):333–341, 2020.

[17] Huaiyuan Gu, Ronald C. Cheung, Fintan Healy, Djamel Rezgui, Mark H. Lowenberg, and Jonathan E. Cooper. Experimental study of the impact of folding wingtip devices on aircraft flight mechanics and handling qualities. *AIAA SCITECH 2023 Forum*, 2023.

[18] Gaétan X. Dussart, Sezsy Y. Yusuf, and Mudassir Lone. Identification of in-flight wingtip folding effects on the roll characteristics of a flexible aircraft. *Aerospace*, 2019.

DOI: 10.13009/EUCASS2023-915

[19] Fintan Healy, Ronald C. Cheung, Theodor Neofet, Mark H. Lowenberg, Djamel Rezgui, Jonathan E. Cooper, Andrea Castrichini, and Tom Wilson. Folding wingtips for improved roll performance. *AIAA Scitech 2021 Forum*, 2021.

[20] J.R.Wright and J. E.Cooper. *Introduction to aircraft aeroelasticity and loads*. John Wiley and Sons Ltd, 2^{nd} edition, 2014.

[21] The MathWorks Inc. Matlab version: 9.13.0 (r2022b), 2022.

[22] Michael Cook. *Flight Dynamics Principles: A Linear Systems Approach to Aircraft Stability and Control*. Butterworth-Heinemann, 3^{rd} edition, 2012.